Published in final edited form as:
J Control Release. 2011 October 30; 155(2): 144–151. doi:10.1016/j.jconrel.2011.06.044.

In vivo tumor targeting by a NGR decorated micelle of a recombinant diblock copolypeptide

Andrew J. Simnick[a], **Miriam Amiram**[a], **Wenge Liu**[a], **Gabi Hanna**[b], **Mark. W. Dewhirst**[b], **Christopher D. Kontos**[c], and **Ashutosh Chilkoti**[a,*]

[a]Department of Biomedical Engineering, Duke University, Durham, NC 27708, USA

[b]Department of Radiation Oncology, Duke University Medical Center, Durham, NC 27710, USA

[c]Department of Medicine, Division of Cardiology, Duke University Medical Center, Durham, NC 27710, USA

Abstract

Antivascular targeting is a promising strategy for tumor therapy. This strategy has the potential to overcome many of the transport barriers associated with targeting tumor cells in solid tumors, because the tumor vasculature is directly accessible to targeting vehicles in systemic circulation. We report a novel nanoscale delivery system consisting of multivalent polymer micelles to target receptors that are preferentially upregulated in the tumor vasculature and perivascular cells, specifically CD13. To this end we utilized amphiphilic block copolymers, composed of a genetically engineered elastin-like polypeptide (ELP) that self-assemble into monodisperse spherical micelles. These polymer micelles were functionalized by incorporating the NGR tripeptide ligand, which targets the CD13 receptor, on their corona. We examined the self-assembly and *in vivo* tumor targeting by these NGR-functionalized nanoparticles and show that multivalent presentation of NGR by micelle self-assembly selectively targets the tumor vasculature by targeting CD13. Furthermore, we show greater vascular retention and extravascular accumulation of nanoparticles in tumor tissue compared to normal tissue, although the enhancement is modest. These results suggest that enhanced delivery to solid tumors can be achieved by targeting upregulated receptors in the tumor vasculature with multivalent ligand presenting nanoparticles, but additional work is required to optimize such systems for multivalent targeting.

Keywords

Drug delivery; Tumor; Thermally responsive polymer; Elastin-like polypeptide

1. Introduction

Hydrophilic polymer carriers have gained much attention in the past few decades for the delivery of anti-cancer agents to solid tumors because they can: (1) increase the solubility of hydrophobic drugs; (2) increase their plasma half-life; (3) increase accumulation of drug in

*Corresponding author Tel.: 11-919-660-5373; fax: 11-919- 660-5362; chilkoti@duke.edu.

tumor; (4) reduce their accumulation in healthy organs and thereby reduce systemic toxicity; and can (5) allow incorporation of targeting moieties [1, 2]. While initial research in this area focused on polymer-drug conjugates [3, 4], recent work has focused on amphiphilic block copolymers that can self-assemble into nano-meso scale structures [5–7], which are capable of both sequestering drug and presenting a targeting ligand or a sub-cellular localization signal on their exterior.

We [8, 9] and others [6, 10, 11] are interested in developing block copolymers that self-assemble into amphiphilic nanoscale structures that facilitate the presentation of ligands specific for tumor-associated antigens. In this context, we are particularly interested in using multivalent polymer micelles to target receptors that are preferentially upregulated in the tumor vasculature and perivascular cells. The NGR/aminopeptidase-N (CD13) ligand-receptor system is of particular interest for tumor targeting for the following reasons [12, 13]. First, CD13 is a membrane-bound enzyme that is associated with angiogenic tumor vessels [13, 14]. Second, the NGR peptide has been shown previously to target macromolecular constructs to angiogenic vasculature in tumors through a putative interaction with CD13, making it of interest for targeting antiangiogenic agents to the tumor vasculature [15]. Third, the NGR tripeptide shows low-affinity in linear form suggesting potential benefit to increasing avidity through the multivalency effect [16].

To design a nanoscale delivery system that is capable of targeting CD13, we focused our attention on a class of recombinant repetitive polypeptides termed elastin-like polypeptides (ELPs). ELPs consist of a Val-Pro-Gly-Xaa-Gly repeat (Xaa = any amino acid besides Pro) and exhibit inverse phase transition behavior at a specific transition temperature (T_t); ELPs are soluble in water at $T < T_t$ and become insoluble at $T > T_t$ [17, 18]. We and others have previously shown that diblock ELPs (ELP Block Co-polymers, ELP_{BC}s) consisting of a hydrophilic ELP block and a hydrophobic ELP block are temperature triggered amphiphiles; the ELP_{BC} is a hydrophilic unimer that self-assembles into monodisperse spherical micelles above a critical micelle temperature (CMT) due to selective desolvation and collapse of the hydrophobic block [8, 18, 19]. These ELP_{BC} micelles have several attractive features for the design of macromolecular drug carriers. First, ELP_{BC}s are monodisperse, which provides exquisite control over their size and hence the size and coordination number of the self-assembled supramolecular structure. Second, they can be easily expressed at high levels in *E. coli* and are conveniently purified by inverse transition cycling (ITC) [20], a method that exploits the ELP phase transition to purify them in large quantities directly from cell lysates without chromatography. Third, we have shown that ELP_{BC}s are remarkably tolerant to the presentation of linear peptide ligands at their N-terminus, as we have successfully incorporated linear peptides without disrupting self-assembly [8]. Fourth, we have shown that micelle self-assembly enables multivalent presentation of these linear peptides for high affinity targeting of cell surface receptors [9]. These advantages make ELP_{BC}s a useful system for developing ligand-functionalized nanoparticles for drug delivery and provide the motivation for this study.

Herein, we report on the ability of multivalent NGR-functionalized ELP_{BC} nanoparticles to target CD13 in the tumor vasculature following systemic administration. We examined the self-assembly properties using dynamic light scattering (DLS) and used two different methods – intravital laser scanning confocal fluorescence microscopy (ILSCFM) and immunofluorescence (IF) – to examine *in vivo* tumor targeting by these NGR-functionalized nanoparticles. Each of these approaches provided insights into different aspects of tumor accumulation of ELP_{BC}s. ILSCFM of tumors implanted in a dorsal skin-fold window chamber provided qualitative data regarding the spatial distribution and quantitative data regarding plasma half-life, accumulation, and extravasation of the micelle in the tumor. IF provided a complementary methodology that was useful in identifying colocalization of the

NGR-ELP_{BC} with specific histological markers present in the tumor. To the best of our knowledge, with the exception of a recently published study by Allen and co-workers [21], this is the first study that quantifies the real-time 3-D accumulation of both functionalized and non-functionalized monodisperse polymeric micelles, and the findings of these studies have implications for the field of vascular targeting of tumors using this class of peptide ligand.

2. Materials and Methods

2.1. Nomenclature

ELPs are described by the nomenclature $ELP[V_xA_yG_z]_m$, where m refers to the number of pentapeptide repeats and x, y, and z refer to the relative fraction of valine, alanine, and glycine in the guest residue position along the length of the protein. The block copolymers used in this study have the composition $ELP[V_1A_8G_7]_m/ELP[V]_m$ which we abbreviate as (ELP-m/n) where m = 64 and n =90.

2.2. ELP Cloning and Expression

The gene encoding the ELP-64/90 block copolymer was available from a previous study [18], and was modified to incorporate the NGR motif as follows. Unmodified pET-25b plasmid (Novagen, Madison, WI) was digested with EcoRI and NdeI (New England Biolabs, Ipswich, MA) and purified using a gel extraction kit (Qiagen, Valencia, CA). Synthetic oligonucleotides encoding the sense and antisense strands of the N-terminal leader and C-terminal trailer peptide sequences in the ELPs (IDT, Coralville, IA) were annealed to form a cassette with EcoRI and NdeI compatible ends (Supplementary information, Fig. S1). These cassettes were ligated into EcoRI and NdeI digested pET-25b and transformed into Top10™ competent cells (Invitrogen, La Jolla, CA) to generate the modified expression vectors, pET-25bAS6 and pET-25bSV2 (Supp. Figure S1). Following confirmation by DNA sequencing, the pET-25bAS6 and pET-25bSV2 vectors were digested with SfiI (New England Biolabs) and purified by gel purification. The ELP-64/90 gene was ligated into the modified pET-25b vector and transformed into BLR competent cells (Novagen, Madison, WI). Successful ligation was confirmed by restriction digestion with XbaI and HindIII (New England Biolabs) and DNA sequencing. All successful clones were stored as frozen stocks at −80 °C until further use.

2.3. ELP Purification

All ELPs used in this study were expressed by a hyperexpression protocol [20]. BLR *E. coli* transformed with the modified pET-25b expression vector that harbored the gene for the diblock ELP_{BC} of interest were grown overnight in a shaker incubator in 50 mL TB Dry™ media (Mo Bio Laboratories, Inc., Carlsbad, CA) and 1 mg/mL ampicillin at 37 °C and 270 rpm. The next day, the cultures were centrifuged to collect the cells and the cells were then resuspended in 1 L TB™ Dry media with 1 mg/mL ampicillin at 37 °C and 270 rpm. The cells were harvested and lysed by ultrasonication, and the ELP_{BC}s were then purified by inverse transition cycling (ITC) [20]. Each ELP was purified from the soluble fraction of cell lysate by 5 rounds of ITC and resuspended in PBS. ELP purity was qualitatively monitored by SDS-PAGE and ELP concentration was measured by UV-Vis spectroscopy using an extinction coefficient of 5690 $M^{-1}cm^{-1}$ [22] for both NGR-ELP64/90 and ELP64/90. ELP stocks were stored at −20 °C until further use.

2.4. Fluorophore Conjugation

1 mL of 200 μM ELP_{BC} was pelleted by centrifugation at 16000×*g* at 50 °C, a temperature that is above the T_t of the ELP. The resulting pellet was resuspended in 900 μL conjugation

buffer (0.1 M $NaPO_4$, 3 mM tris(2-carboxyethyl) phosphine hydrochloride, Thermo Scientific, Waltham, MA) at room temperature. 1 mg of AlexaFluor488-C5 maleimide (AF488, Invitrogen, Carlsbad, CA) was then dissolved in 100 μL anhydrous dimethyl sulfoxide (Sigma-Aldrich, St. Louis, MO), immediately mixed with ELP in its binding buffer, and continuously rotated at RT. The reaction was quenched after 2 h by adding 5 M NaCl solution to precipitate ELP_{BC}, and excess fluorophore was removed by one round of ITC and desalted on a PD-10 gel-filtration column (GE Healthcare, Waukesha, WI). The ELP-AF488 conjugate was concentrated to 1 mL total volume by ITC, and stored at −20 °C. The ELP concentration was measured by UV-Vis spectroscopy (Nanodrop; Thermo Scientific) using the equation:

$$C_{ELP-AF\ 488} = \frac{Abs_{280} - .11 * Abs_{495}}{5690} \quad (1)$$

and the conjugation efficiency was measured using the equation:

$$Eff = \frac{C_{AF\ 488}}{C_{ELP}} \quad (2)$$

with C_{AF488} determined using an extinction coefficient of 71000 cm^{-1} M^{-1} (Invitrogen conjugation manual) at 495 nm.

2.5. Dynamic Light Scattering

100 μL of 10 μM ELP_{BC}-AF488 in PBS was filtered using a 0.02 μm syringe filter (GE Healthcare) and 35 μL of the filtered solution was added to each well of a 384-well plate (Corning, Corning, NY). Small drops of mineral oil were added to the top of each well to prevent evaporation. Samples were analyzed using a thermally controlled dynamic light scattering Wyatt Plate Reader (Wyatt Technology, Santa Barbara, CA). Ten acquisitions were obtained for each well in 1 °C increments from 20 – 45 °C. The resulting data were analyzed using a Rayleigh sphere model and fitted using either a regularization or cumulant algorithm based on the sum-of-squares value. The Rayleigh sphere model was used as ELP_{BC} micelles form monodisperse nanospheres following self-assembly [8] Populations comprising less than 2% of the total mass were excluded from the analysis. These data were used to directly determine the average hydrodynamic ratio (R_h) of the particles in solution. The critical micelle temperature (CMT) for each construct was defined as the lowest temperature at which the R_h is significantly greater than the average unimer R_h.

2.6. Thermal Characterization in Serum

NGR-ELP-64/90 and ELP-64/90 (negative control) were added to fetal bovine serum (FBS; Sigma-Aldrich) at a concentration of 10 μM. 750 μL of each solution were added to a reduced-volume quartz cuvette and analyzed on a thermally controlled UV-Vis spectrophotometer (Cary 300 Bio; Varian, Inc., Cary, NC). The absorbance at 350 nm ($O.D._{350}$) was zeroed at 15 °C and monitored from 15 – 55 °C in 0.33 °C increments. The data were corrected to separate the effects of protein settling from micellar self-assembly by applying a linear fit to data from 15 – 25 °C (Igor Pro; WaveMetrics, Inc., Lake Oswego, OR). This fit was subtracted from the raw data to set a baseline. The temperature at which the corrected $O.D._{350}$ increased beyond the corrected baseline was defined as the CMT.

2.7. RT-PCR

Nude mice (n=2, BALB/c nu/nu, female, BW = 20 ± 3 g; Charles River Laboratories, Wilmington, MA) were housed in a pathogen-free environment in the Duke University Main Vivarium. Tumor leg xenografts were established from a human squamous cell carcinoma (FaDu) tumor cell line. FaDu cells were cultured as a monolayer in tissue culture flasks in culture medium containing minimal essential medium (MEM) supplemented with Earle's salts, L-glutamine, 10% heat-inactivated FBS, 100 U/ml penicillin, 100 μg/ml streptomycin and 0.25 μg/ml amphotericin B (Gibco). The right lower leg of each mouse was implanted s.c. with 1×10^6 cells in 30 μl of MEM Medium without serum. Mice were anesthetized with Phenobarbital (82 mg/kg) and established tumors (150 ± 20 mm^3) were removed. Likewise, muscle tissue was collected from the left leg (without tumor) of the same mice. The mice were sacrificed via cervical dislocation. All tissue samples were immediately frozen in liquid nitrogen and kept at -80 °C before RNA extraction.

Before RNA extraction, tissue samples (120±10mg) were placed in 2ml tubes filled with 1800 μl of buffer RLT (Qiagen) and ~30 2 mm zirconia beads (Biospec, Bartlesville, OK). Tissues were homogenized by disruption for 1 min on a Mini-Beadbeater (Biospec, Bartlesville, OK). Total RNA was purified from homogenized tissues with the RNeasy plus mini kit (Qiagen) according to the manufacturer's instructions. Typically, the yield of RNA from tumor tissue was 20-fold higher than the yield of RNA from muscle tissue. To generate cDNA, RNA was reverse transcribed with random primers using the QuantiTect reverse transcription Kit (Qiagen) according to the manufacturer's instructions and was diluted 10-fold before use in PCR reactions.

For specific gene amplifications, primers sequences were: ITGAV-F: TCGGGACTCCTGCTACCTCTG; ITGAV-R: CACGAGAAGAAACATCCGGGAA; ITGB3-F: TCACCAGTAACCTGCGGATTG; ITGB3-R: GTAGCCAAACATGGGCAAGC; CD13-F: CAGGGGCCTGTACGTTTTTA; CD13-R: CTCGAACTCGCTGTCCATCTCATA; beta-actin-F: GGCTGTATTCCCCTCCATCG; beta-actin-R: CCAGTTGGTAACAATGCCATGT. For PCR reactions, 25 μl solutions were prepared containing 12.5 μl GoTaq green master mix (Promega), 10 pmol gene-specific forward and reverse primers, and either 5 μl of cDNA mixture, non-transcribed RNA mixture (to check for DNA contamination in RNA samples), or nuclease-free water (water control). The PCR reaction conditions were: 95 °C for 2 min, followed by 35 cycles at 95 °C for 20 s, 60 °C for 20 s, and 72 °C for 40 s. The results were visualized on a 2% agarose gel. Correct gene amplification was verified by DNA sequencing (ETON bioscience Inc.) and subsequent alignment of the sequenced DNA with the reported nucleotide sequences of human ITGAV, ITGB3, CD13 and murine beta-actin confirmed correct amplification.

2.8. Dorsal-Fold Window Chamber Surgery

Nude mice (BALB/c nu/nu, female, BW = 20 ± 3 g; Charles River Laboratories, Wilmington, MA, n=3) were housed in a pathogen-free environment in the Duke University Main Vivarium. After one week, a titanium window chamber was surgically affixed to the dorsal skin fold of each mouse. Briefly, each mouse was anesthetized using intraperitoneal (*i.p.)* injection of 100 mg/kg ketamine and 10 mg/kg xylazine. The skin fold was cleaned and stretched, and a 1 cm circular incision was made on one side of the fold. The window chamber plates were then affixed around the incision. For tumor analysis, 10 μL of FaDu cells suspended in serum-free DMEM at 4×10^6 cells/mL were injected subcutaneously into the skin within the window chamber. For normal tissue analysis, this step was not performed. The window chamber was then sealed with a glass cover slip and additional sutures. Mice were then housed for 7–10 days at which time the implanted tumor was typically 2–3 mm in diameter.

2.9. Confocal Imaging

Nude mice (BALB/c nu/nu) with implanted dorsal fold window chambers were anesthetized with *i.p.* injection of sodium pentobarbital (80 mg/kg) and positioned in lateral recumbency on a heated, custom-designed microscope stage (Supplementary information, Fig. S3). The tail vein was cannulated for intravenous (*i.v.*) administration of an ELP_{BC} or anesthesia. The window chamber was fixed to the microscope stage to limit three-dimensional translation (in x-, y-, and z-directions, where z corresponds to the axial direction). Fluorescence images were acquired using a LSM510 laser scanning confocal microscope (Zeiss, Jena, Germany) with an in-plane resolution of 512 × 512 pixels and a field of view of 460 μm × 460 μm.

A dual-color imaging routine consisting of line switching between green and red detection was used to obtain vessel images (red) and images of ELP_{BC} (green). The pinhole size corresponding to a slice thickness of 7.1 μm was selected for both channels, and the gain of each channel was increased until autofluorescence was detected from the tissue. A background image was then obtained, prior to injection of any fluorescent compound. 100 μL of 1 mg/mL 2 MDa MW dextran-rhodamine (Invitrogen) was then administered by the cannula and observed using a fast XY scan. The region of interest (ROI) was centered using the XY translational stage and the upper and lower limits of the tumor volume were set as bounds for the z-stack, and a single z-stack of the contrast agent was obtained to identify the plasma compartment. 100 μL of 141 μM ELP_{BC} was then administered via the cannula immediately followed by an imaging routine consisting of 20 z-stacks over 45 min. 40 μL of 80 mg/kg sodium pentobarbital was administered 40 min following the initial anesthesia dose and 20 μL every subsequent 20 min. Following imaging, the mouse was sacrificed.

2.10. Image Processing

Raw data from each imaging routine was exported offline to an image processing workstation containing both the LSM imaging software (Zeiss) and MATLAB equipped with the Image Processing toolbox (The Mathworks, Natick, MA). The image stack was separated into individual channels representing ELP and vessel contrast agent. The image series from each channel were exported to MATLAB as a structure of '.tif' files. Images corresponding to vessel contrast agent were manually motion-corrected in the x, y, and z directions at three distinct locations in the image and checked for accuracy. The z-stack of the contrast agent at the initial time point was then used to generate a 3D binary mask separating the vascular and extravascular regions. The resulting binary mask was used to generate a 3D map defining the distance of each voxel from the nearest vessel surface in the x, y, and z directions within the ROI. Motion-corrected data corresponding to ELP_{BC} was then directly applied to the binary mask to obtain time-dependent accumulation data in the vascular and extravascular compartments and applied to the distance map to obtain time-dependent extravasation data.

2.11. Histological Staining

Nude mice (BALB/c nu/nu, female, BW = 20 ± 3 g, n=3) were housed in a pathogen-free environment in the Duke University Main Vivarium. FaDu xenografts were implanted on the hind legs by subcutaneous injection of 10^6 cells and allowed to grow for 10 days. Mice were injected with NGR-ELP-64/90-AF488 or ELP-64/90-AF488 at a plasma concentration of 10 μM and maintained at 37 °C. After 1 h, 50 μL of 10mg/mL Hoechst 33342 dye was administered via *i.v.* injection. After 1 minute, the mouse was sacrificed by cervical dislocation. Tumor tissue and the opposing leg muscle were immediately excised. Each tissue was embedded in tissue freezing medium (TBS, Durham, NC) and snap-frozen in liquid nitrogen. Slices of tumor and normal tissue were cut into 15 μm-thick sections using a manual cryotome (Leica Microsystems, Bannockburn, IL). Unfixed slides were kept on dry ice or at −80°C until further use.

Each slice was imaged to detect both ELP-AF488 and Hoechst 33342 using a scanning-stage epifluorescence microscope (Nikon Instruments, Tokyo, Japan) within 24 hours of being mounted on a slide. Slides were then rinsed in blocking buffer (10% BSA), stained with either primary anti-CD31 antibody or primary anti-rat IgG2 (negative control), rinsed again, and stained with secondary anti-mouse IgG labeled with AlexaFluor 546 (Invitrogen). Each slide was then immediately reimaged using scanning-stage epifluorescence microscopy to detect the AlexaFluor 546 signal. The images obtained prior to antibody staining and post-antibody staining were overlaid using Photoshop (Adobe, San Jose, CA).

3. Results

3.1. ELP_{BC} Design, Expression and Physical Characterization

We designed an NGR-ELP_{BC} using an existing gene for ELP-64/90. This diblock ELP_{BC} encoded four contiguous segments: a hydrophilic ligand (NGR), a flexible GGS peptide linker, a hydrophilic ELP segment and a hydrophobic ELP segment followed by a trailer peptide (WPC) for conjugation of fluorophore or drug to the Cys (C) residue. The ELP-64/90 diblock copolymer was successfully expressed with a yield of 200 mg/L of culture. SDS-PAGE showed that the resulting ELP_{BC} unimers had the expected MW as seen by a primary band at approximately 60 KDa for ELP-64/90 (Figure 1). The faint secondary band in SDS-PAGE was twice as large as the size of the intense band and was the only other band on the gel, suggesting that it is a result of dimer formation caused by the presence of the Cys residues at the C-terminus. We conjugated both ELP_{BC}s to AlexaFluor488 at a conjugation ratio > 70% and measured the critical micelle temperature (CMT) of 10 μM ELP_{BC} in serum using UV/Vis-spectroscopy. The CMT of NGR-ELP-64/90 and ELP-64/90 were 31°C and 32°C, respectively, suggesting that the ELP_{BC} will self-assemble into micelles in serum at normothermia (Supp. Figure S5).

3.2. Dynamic Light Scattering Characterization

Prior to cell uptake experiments, we characterized the thermally triggered self-assembly of NGR-ELP_{BC} that was conjugated with AlexaFluor 488 at its C-terminus (NGR-ELP-64/90) and a ligand-negative control (ELP-64/90) in aqueous solution by temperature-programmed dynamic light scattering (DLS). Both ELP_{BC}s were conjugated to AlexaFluor 488 at a conjugation ratio of > 70%. We measured the hydrodynamic radius (R_h) of a 10 μM ELP_{BC} solution as a function of solution temperature by DLS from 20 °C – 45 °C (Figure 2). This concentration range was chosen as it was higher than the calculated CMC for unmodified ELP-64/90 (8.1 μM) [8], but is sufficiently dilute for DLS measurement, and compatible with *i.v.* administration. Both ELPs exhibited two phases: (1) a soluble unimer phase with an R_h = 5–8 nm at T < critical micelle temperature (CMT) and (2) a nanoparticle with R_h = 25–30 nm at T > CMT. In both cases, the pattern of self-assembly was similar, with a 6–8 ºC temperature range in which the micelles were stable. Additionally, there was only one detectable population for each ELP_{BC} at all temperatures indicating that self-assembly proceeded nearly to completion at these concentrations.

The DLS measurements also showed that the CMT of ELP-64/90 was 34 °C following conjugation of AF488, and the presentation of NGR at the hydrophilic terminus of the micelle lowered the CMT by 5 °C to 29 °C (Figure 2). These results showed that the CMT of ELP-64/90 and of NGR-ELP-64/90 were both below 37 ºC and thus would retain self-assembly at physiologic temperature.

3.3. In Vivo Analysis Using the Dorsal Fold Window Chamber Model

We next examined the binding and uptake of the NGR-ELP_{BC} in a s.c implanted tumor using intravital laser-scanning confocal microscopy (ILSCM). We chose ILSCM because it

allows real-time imaging of an implanted tumor and quantification of the kinetics and spatial distribution of fluorescently labeled drug carriers within a tissue of interest that is implanted in the window chamber. We used ILSCSM specifically to compare the effect of multivalent NGR presentation on the accumulation of NGR-ELP_{BC} micelles and ligand-negative controls in both tumor and normal tissue.

Having established that FaDu tumors are CD13+ positive, (see SI and Supplemental figure S2), we next carried out ILSCFM to visualize and quantify the effect of NGR presentation on the spatial distribution and accumulation of the ELP_{BC} within the tumor. FaDu tumors in the window chamber were first imaged at low magnification to qualitatively visualize the spatial distribution of blood vessels. Fluorescent ELP_{BC} constructs were then administered by tail-vein injection, and accumulation of the ELP_{BC}s was viewed at higher magnification at different locations in the tumor. Under the experimental conditions utilized for these studies, both ELP_{BC}s exist as micelles. The central low-magnification image shows the tumor vasculature prior to ELP-64/90 administration (red), and the high-magnification images show ELP-64/90 accumulation 45 min after systemic administration of the ELP (green) (Figure 3). There were clear differences in the spatial distribution of each construct. ELP-64/90, the ligand-negative control micelle, showed very little punctate fluorescence in any vessels within the vasculature. There was no visible difference in accumulation in smaller or larger tumor vessels. In contrast, NGR-ELP-64/90 exhibited a different spatial localization than ELP-64/90. There was enhanced punctate fluorescence in the central immature vessels, but low levels of accumulation in larger peripheral vessels. There was also enhanced extravasation from the larger feeder vessels at the tumor margin. These results showed that multivalent presentation of NGR affects accumulation differently in different regions of the vasculature. However, both ligand- and non-ligand ELP_{BC} extravasated from vessels at the tumor periphery.

Based on the spatial distribution of the two ELP_{BC}s, we chose to analyze smaller vessels within the central tumor regions. We monitored the accumulation of ELP-64/90 and NGR-ELP-64/90 in the intravascular and extravascular regions, as defined by the binary mask. The detected fluorescence intensity in each compartment was normalized to the intensity immediately following administration of the fluorescent ELP_{BC}. This normalized intensity represented the percent of the initial dose (% ID) and was used to measure the amount of the ELP_{BC} in each compartment as a function of time as follows: we quantitatively evaluated accumulation in the vascular compartment to: (1) determine the effects of multivalent ligand presentation on clearance; and (2) estimate plasma concentration of the ELP_{BC}s over the time course of imaging (Figure 4). ELP-64/90 showed more rapid clearance from the normal vasculature than tumor vasculature in the first half of the time course, and the concentration reached approximately 50 – 60% ID in both tumor and normal vasculature after 1 h. Similarly, NGR-ELP-64/90 showed more rapid clearance from normal vasculature than tumor vasculature, which was true over the entire time course. However, the vascular concentration was ~80% ID in the tumor vasculature at the 45 min time point, compared to ~50% ID in the normal vasculature.

These data provide several insights regarding the effect of multivalent presentation of the NGR ligand on vascular targeting of the ligand. Assuming an initial plasma concentration of 10 μM, the observed % ID indicates that both ligand and non-ligand ELP_{BC} circulate as micelles, which is supported by the finding that the ELP_{BC}s self-assembled into micelles in serum at both 10 μM and 5 μM (Supplementary information, Fig. S4 and S5). The greater accumulation of the NGR-decorated micelles in the vascular space compared to the control, unmodified micelles, suggests the specific interaction of NGR-ELP-64/90 with a vascular component in the tumor vasculature following systemic administration that is related to the presence of the NGR ligand.

Second, we used the window chamber to quantify the effect of ligand presentation on extravascular accumulation in both tumor and normal tissue (Figure 4). Both constructs led to increased % ID in both tumor and normal tissues over the time course of observation. ELP-64/90 showed a slight increase in its accumulation in tumor tissue (2 – 3 fold) compared to surrounding normal tissue (1.5 – 2.5 fold). In contrast, NGR-ELP-64/90 showed a greater increase in accumulation in tumor tissue (3 – 4 fold) compared to normal tissue (1 – 2 fold) over the experimental time course. This difference suggests that the presentation of NGR-ELP-64/90 significantly improved the degree of accumulation within the central extravascular tumor region.

3.4. Immunofluorescence

One limitation of the window chamber is its insufficient resolution to separate different cell types within the perivascular region. Hence, we next used Immunoflourescence (IF) microscopy to characterize the binding of NGR-ELP-64/90 and ELP-64/90 to different cell types in tumor and normal tissues to independently verify the window chamber results over a larger ROI and further identify the binding site of NGR-ELP-64/90. Mice with a hind leg FaDu xenograft were administered a dose of either NGR-ELP-64/90 or ELP-64/90 (green) at 10 μM plasma concentration. After 1 hour, mice were administered Hoechst 33342 solution *i.v.* to stain perfused vessels (blue) and were immediately sacrificed. The tumor and opposing leg muscle were removed, sectioned, and stained for CD31 expression (red) to identify endothelial cells (Figure 5).

Stained tissue slices showed that there was greater green fluorescence from tumors explanted from animals dosed with NGR-ELP-64/90 than ELP-64/90. Punctate green fluorescence corresponding to NGR-ELP-64/90 overlapped with perivascular cells. Conversely, it was weakly present in these regions following administration of the ligand negative control micelle of ELP-64/90. In contrast, there was visible green fluorescence in normal tissue for both ELP_{BC}s. The green fluorescence was more intense for NGR-ELP-64/90 than ELP-64/90 in regions associated with CD31 expression, but neither nanoparticle showed punctate fluorescence in tissue sections from normal tissue. These histological images confirmed patterns of accumulation as described by the window chamber with greater accumulation of NGR-ELP-64/90 in tumor regions but similar accumulation in normal tissue, and they suggest that NGR-ELP-64/90 has the potential to improve vascular targeting of constructs in the central tumor region.

4. Discussion

The results presented herein show that multivalent presentation of NGR by ELP_{BC} self-assembly selectively targets tumor vasculature through the effect of multivalent targeting of CD13. Analysis of the dorsal fold window chamber images acquired by ILSCFM showed greater vascular retention and extravascular accumulation of NGR-ELP_{BC} constructs in tumor tissue compared to normal tissue. In contrast, this effect was not observed with non-ligand ELP_{BC} constructs. Histological staining supported these observations by showing increased NGR-ELP-64/90 fluorescence in tumor regions corresponding to endothelial and perivascular cells, an effect that was not seen with ELP-64/90. Further evaluation of the binding sites using quantitative histology or colocalization studies using ILSCFM may reveal binding sites beyond endothelial cells. As CD13 is expressed on cell types such as lymphocytes and distressed pericytes, identification of the exact binding sites may reveal the mechanism promoting specificity for the tumor region.

There are several attractive features of multivalent targeting of the tumor vasculature that provide an impetus for future study of its mechanism and its translation to a therapeutic application. First, binding to the tumor vasculature is attractive for targeting as the tumor

vasculature, including endothelial cells and pericytes, are ubiquitous to all solid tumors and potentially circumvents the need to target genomically unstable tumor cells. Second, directly targeting the vasculature circumvents the limited penetration of nanoparticles into interstitial space of solid tumors [23]. Third, the genetically encoded synthesis of NGR-ELP_{BC} allows easy generation of ligand-presenting micelles and potentially mixed micelles of NGR-decorated ELP_{BC}s with unmodified ELP_{BC}s to titrate the valency of the micelles.

Nevertheless, much remains to be done before this system would be useful for *in vivo* targeting. First, it would be desirable to increase the degree of accumulation of the NGR decorated micelles. This may be possible by titrating the number of NGR ligands on the surface, as overcrowding of ligands can lead to steric hindrance, and hence impaired ligand – receptor binding [24]. Second, the accessibility of the ligand may require tethering the NGR ligand away from the corona using a flexible peptide spacer to allow conformational sampling of the receptor-binding site.

While these strategies may provide a further degree of improvement in tumor vasculature targeting that we believe will be clearly necessary to translate this targeting modality to the clinic, there remains the distinct possibility that multivalent receptor targeting may have an Achilles heel that has generally not been adequately addressed. Because multivalent targeting requires the engagement of multiple ligands simultaneously with multiple receptors, the surface density of receptors on the cell surface and their spatial clustering is critical to achieve the amplification in apparent affinity (avidity), a prospect that has made multivalent ligand-receptor interaction an attractive approach for targeted drug delivery. However, it is not entirely clear whether the tumor vasculature has the necessary receptor density and clustering necessary for this approach to work.

This lacuna in our knowledge needs to addressed, in our opinion, by carrying out systematic studies of multivalent targeting in well-defined, yet clinically relevant animal models in which the density of both ligands and of receptors is systematically varied. Doing so poses two requirements: first, creating nanoparticles in which the surface density of a ligand of interest can be systematically varied, which we note is easily possible using the ELP_{BC} based nanoparticle system described herein and by other synthetic polymer nanoparticles [6, 9]. The second and greater challenge is the development of tumor models in which the receptor density can be similarly titrated in the tumor vasculature (for vascular targeting) or tumor cells. Generating such engineered, tunable systems for ligand presentation and *in vivo* receptor presentation on solid tumors is clearly necessary to rationally develop this, and other multivalent targeting systems for clinical application.

5. Conclusion

Multivalent presentation of an NGR peptide ligand by self-assembled polypeptide micelles is shown to selectively target the tumor vasculature by multivalent targeting of CD13 and to increase the delivery of the micelles to tumors compared with non-functionalized micelles. Analysis of the dorsal fold window chamber images acquired by ILSCFM showed greater vascular retention and extravascular accumulation of NGR-ELP_{BC} constructs in tumor tissue compared to normal tissue. Concurrently, histological staining showed increased NGR-ELP-64/90 fluorescence in tumor regions corresponding to endothelial and perivascular cells compared to the ligand-negative micelle control, ELP-64/90 accumulation. Despite these encouraging preliminary results, this targeting system is far from optimized; the current enhancement of tumor accumulation exhibited by multivalent targeting is modest, so that further optimization is clearly necessary by optimizing the number of ligands on the surface of the particle, and possibly by incorporating a flexible spacer to allow for better interaction with cell-surface receptors.

Supplementary Material

Refer to Web version on PubMed Central for supplementary material.

Acknowledgments

We thank Dr. Jun Chen for her guidance on immunostaining technique and Dr. C. Alexander Valencia for his advice on cell-based assays. This work was funded by NIH 5R01 EB 007205.

References

1. Duncan R. Polymer conjugates as anticancer nanomedicines. Nat Rev Cancer. 2006; 6(9):688–701. [PubMed: 16900224]
2. Kopecek J, et al. HPMA copolymer-anticancer drug conjugates: design, activity, and mechanism of action. Eur J Pharm Biopharm. 2000; 50(1):61–81. [PubMed: 10840193]
3. Duncan R. Drug-polymer conjugates: potential for improved chemotherapy. Anticancer Drugs. 1992; 3(3):175–210. [PubMed: 1525399]
4. Duncan R. Polymer conjugates as anticancer nanomedicines. Nature Reviews Cancer. 2006; 6(9): 688–701.
5. Discher DE, Eisenberg A. Polymer vesicles. Science. 2002; 297(5583):967–73. [PubMed: 12169723]
6. Kataoka K, Harada A, Nagasaki Y. Block copolymer micelles for drug delivery: design, characterization and biological significance. Adv Drug Deliv Rev. 2001; 47(1):113–31. [PubMed: 11251249]
7. Kwon GS, Kataoka K. Block-Copolymer Micelles as Long-Circulating Drug Vehicles. Advanced Drug Delivery Reviews. 1995; 16(2–3):295–309.
8. Dreher MR, et al. Temperature triggered self-assembly of polypeptides into multivalent spherical micelles. Journal of the American Chemical Society. 2008; 130(2):687–694. [PubMed: 18085778]
9. Simnick AJ, et al. Morphing Low-Affinity Ligands into High-Avidity Nanoparticles by Thermally Triggered Self-Assembly of a Genetically Encoded Polymer. Acs Nano. 2010; 4(4):2217–2227. [PubMed: 20334355]
10. Kakizawa Y, Kataoka K. Block copolymer micelles for delivery of gene and related compounds. Advanced Drug Delivery Reviews. 2002; 54(2):203–222. [PubMed: 11897146]
11. Rosler A, Vandermeulen GW, Klok HA. Advanced drug delivery devices via self-assembly of amphiphilic block copolymers. Adv Drug Deliv Rev. 2001; 53(1):95–108. [PubMed: 11733119]
12. Buehler A, et al. cNGR: A novel homing sequence for CD13/APN targeted molecular imaging of murine cardiac angiogenesis in vivo. Arteriosclerosis Thrombosis and Vascular Biology. 2006; 26(12):2681–2687.
13. Pasqualini R, et al. Aminopeptidase N is a receptor for tumor-homing peptides and a target for inhibiting angiogenesis. Cancer Research. 2000; 60(3):722–727. [PubMed: 10676659]
14. Bhagwat SV, et al. CD13/APN is activated by angiogenic signals and is essential for capillary tube formation. Blood. 2001; 97(3):652–659. [PubMed: 11157481]
15. Ruoslahti E. Targeting tumor vasculature with homing peptides from phage display. Seminars in Cancer Biology. 2000; 10(6):435–442. [PubMed: 11170865]
16. Sutton D, et al. Functionalized micellar systems for cancer targeted drug delivery. Pharm Res. 2007; 24(6):1029–46. [PubMed: 17385025]
17. Urry DW. Physical chemistry of biological free energy transduction as demonstrated by elastic protein-based polymers. Journal of Physical Chemistry B. 1997; 101(51):11007–11028.
18. Meyer DE, Chilkoti A. Genetically encoded synthesis of protein-based polymers with precisely specified molecular weight and sequence by recursive directional ligation: Examples from the elastin-like polypeptide system. Biomacromolecules. 2002; 3(2):357–367. [PubMed: 11888323]
19. Wright ER, Conticello VP. Self-assembly of block copolymers derived from elastin-mimetic polypeptide sequences. Advanced Drug Delivery Reviews. 2002; 54(8):1057–1073. [PubMed: 12384307]

20. Meyer DE, Chilkoti A. Purification of recombinant proteins by fusion with thermally-responsive polypeptides. Nature Biotechnology. 1999; 17(11):1112–1115.
21. Lee H, et al. The effects of particle size and molecular targeting on the intratumoral and subcellular distribution of polymeric nanoparticles. Mol Pharm. 2010; 7(4):1195–208. [PubMed: 20476759]
22. Gill SC, von Hippel PH. Calculation of protein extinction coefficients from amino acid sequence data. Anal Biochem. 1989; 182(2):319–26. [PubMed: 2610349]
23. Dreher MR, et al. Evaluation of an elastin-like polypeptide-doxorubicin conjugate for cancer therapy. J Control Release. 2003; 91(1–2):31–43. [PubMed: 12932635]
24. Hlavacek WS, Posner RG, Perelson AS. Steric effects on multivalent ligand-receptor binding: exclusion of ligand sites by bound cell surface receptors. Biophys J. 1999; 76(6):3031–43. [PubMed: 10354429]

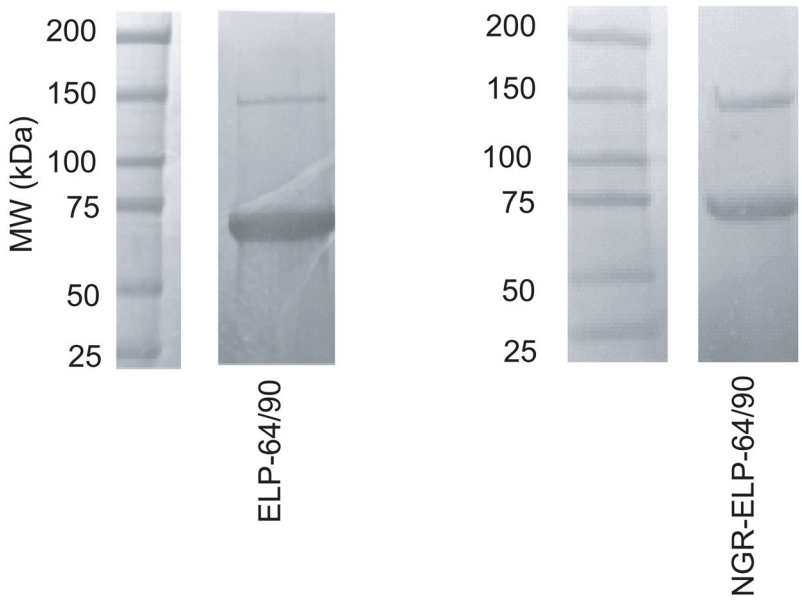

Figure 1.

Expression and purification of NGR-ELP-64/90. SDS-PAGE shows expression of monodisperse ELP_{BC} and purification to near homogeneity. A secondary band was observed at approximately twice the expected size for each ELP_{BC}, likely due to dimerization during purification due to the presence of the Cys residues at their C-terminus.

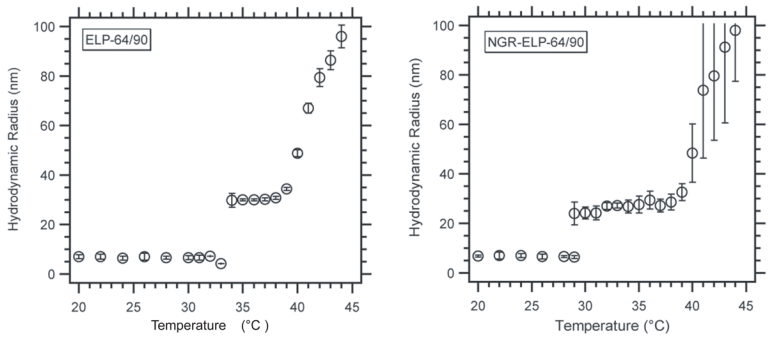

Figure 2.

Hydrodynamic radius of ELP-64/90 and NGR-ELP-64/90 as a function of temperature. All constructs formed monodisperse micelles at a specific temperature defined as CMT. There was a decrease in CMT with the addition of charged NGR ligand.

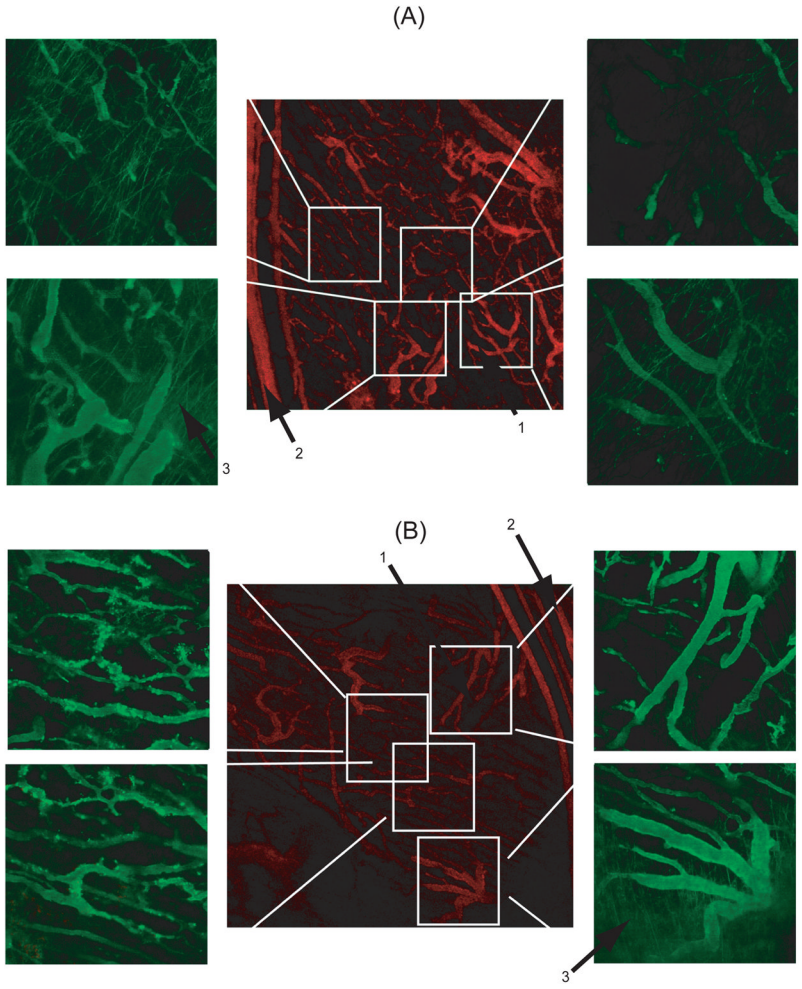

Figure 3.
Spatial distribution of (A) ELP-64/90 and (B) NGR-ELP-64/90 in FaDu tumor xenografts. ELP-64/90 did not show punctate fluorescence in the smaller central vessels and showed extravasation at the tumor periphery. NGR-ELP-64/90 showed punctate fluorescence in central vessels and extravasation at the tumor periphery. Arrow mark (1) smaller central vessels, (2) larger periphery vessels and (3) extravasation pattern.

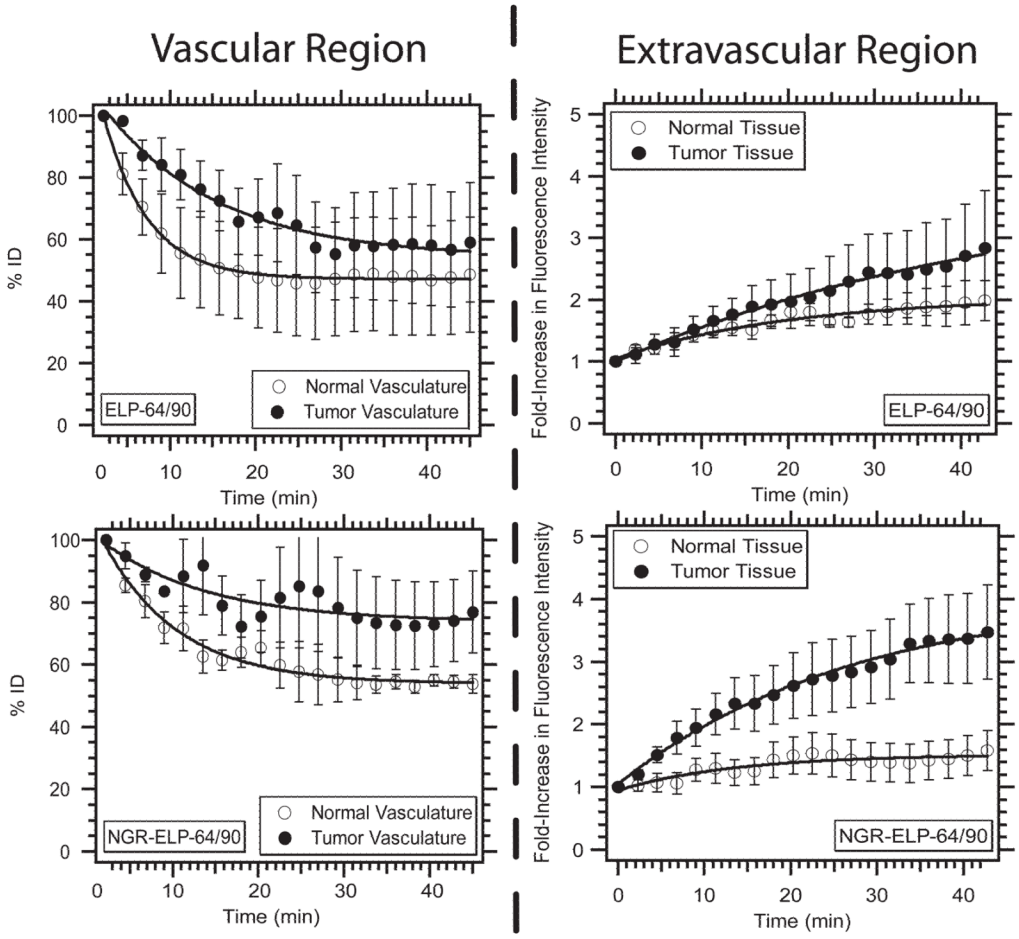

Figure 4.

Relative vascular and extravascular intensity as a function of time. Both NGR-ELP-64/90 and ELP-64/90 decreased in vascular concentration and increased in extravascular concentration. NGR-ELP-64/90 showed greater retention in vasculature and accumulation in the extravascular region compared to ELP-64/90.

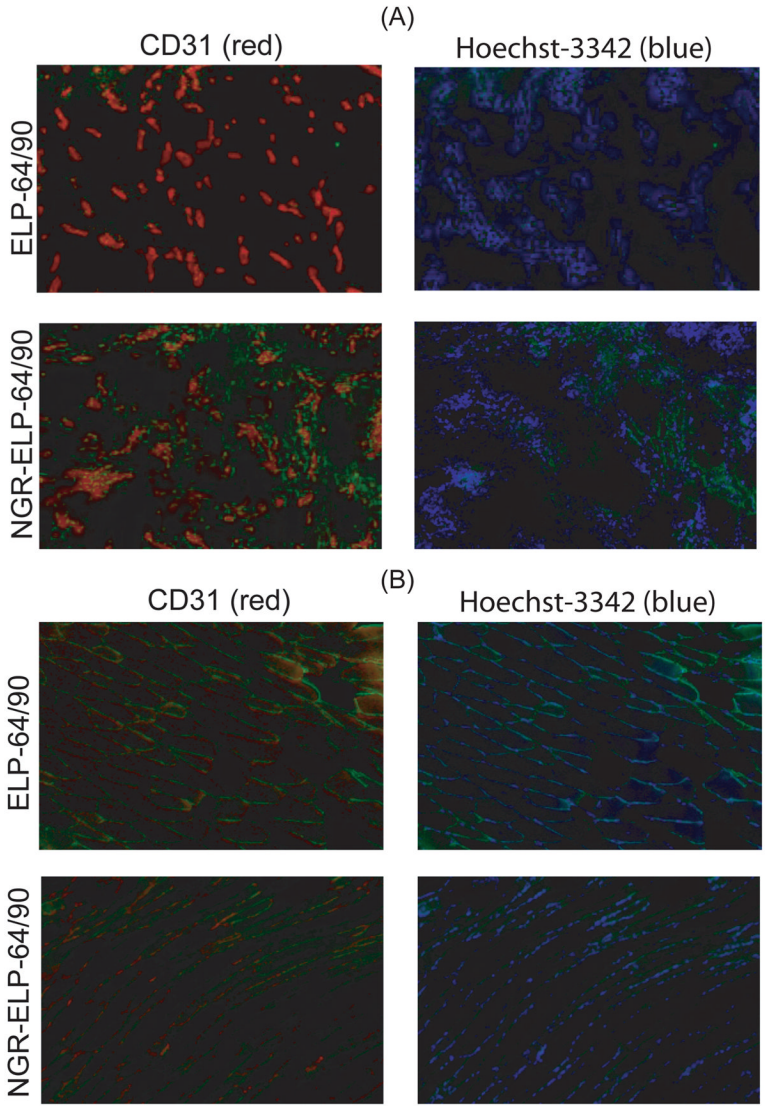

Figure 5.

Immunofluorescence microscopy of tumor and normal tissue following systemic administration of ELP-64/90 and NGR-ELP-64/90. (A) There was a clear increase in fluorescence in the endothelial and perivascular regions of tumor tissue following exposure to NGR-ELP-64/90 but not ELP-64/90. (B) There was less green fluorescence in normal tissue following exposure to NGR-ELP-64/90 than ELP-64/90.